

Incomplete fusion and cluster production in heavy-ion collisions at 30 MeV/nucleon

G. Nebbia, J. A. Ruiz, D. Fabris, and G. Viesti

Istituto Nazionale di Fisica Nucleare Sezione di Padova and Dipartimento di Fisica dell'Università di Padova, I-35131 Padua, Italy

R. H. Burch, F. Gramegna, and G. Prete

Istituto Nazionale di Fisica Nucleare Laboratori Nazionali de Legnaro, I-35020 Legnaro, Italy

A. Giorni, A. Lleres, and J. B. Viano

Institut des Sciences Nucleaires, 38026 Grenoble CEDEX, France

B. Chambon, B. Cheynis, A. Demeyer, D. Drain, D. Guinet, and X. C. Hu

Institut de Physique Nucleaire, 69622 Villeurbanne CEDEX, France

M. Gonin, K. Hagel, J. B. Natowitz, and R. Wada

Cyclotron Institute, Texas A&M University, College Station, Texas 77843

P. L. Gonthier

Department of Physics, Hope College, Holland, Michigan 49423

(Received 7 August 1991)

The total energy dissipated in central collisions has been measured for the system $^{32}\text{S} + ^{58}\text{Ni}$ at about 1 GeV incident energy. An event-by-event reconstruction of the atomic charge of the reaction products was performed by means of a 4π charged-particle detector. Two distinct classes of events were thus separated: one consistent with a "conventional" incomplete fusion-evaporation process, a second where three or more heavy fragments are produced. A subtraction of the evaporative component from the particle spectra at all angles allowed extraction of the excitation energy removed from the system by pre-equilibrium emission. The average excitation energies corresponding to the two different classes of events were determined. Comparisons with statistical model calculations as well as a multifragmentation model are presented.

PACS number(s): 25.70. - z

I. INTRODUCTION

The observation of the properties of very hot nuclei has been the subject of extensive theoretical and experimental work in the last few years [1–7]. There is now available a host of experimental results showing that in intermediate-energy heavy-ion collisions all dissipative processes (fusion-evaporation, fusion-fission, deep-inelastic) become more and more "incomplete" as the relative velocity of projectile and target is increased, the term "incomplete" meaning that the onset of a fast first step in the reactions prevents the system from converting all the available center-of-mass energy into excitation energy.

A variety of possible scenarios have been proposed to describe such fast phenomena, ranging from rather schematic geometrical models (participant-spectator, fireball, etc.) [8] mainly aimed at describing nearly peripheral reactions, to pre-equilibrium models [9] used to describe more central collisions. In all cases there are indications [10,11] that after the first step of the reaction a part of the system reaches thermal equilibrium, but the complexity of the fast processes often results in a rather poor knowledge of the properties of such a hot subsystem such as its excitation energy, temperature, and spin.

In order to characterize quantitatively the production mechanism and the deexcitation properties of the hot nuclei thus formed it is necessary to isolate clearly a part of the total reaction cross section by focusing on a particular class of events.

We present here the results of an experiment in which the reaction of $^{32}\text{S} + ^{58}\text{Ni}$ at 30 MeV/nucleon has been studied. We have selected events where an incomplete fusion process took place, followed by evaporation of only light particles or where such evaporation is accompanied by production of intermediate-mass fragments. In both cases it was imposed that only light particles were emitted in the first stage of the reaction in order to select central collisions. This was done on an event-by-event basis using the 4π charged-particle detector AMPHORA [12]. The selection was performed by reconstructing offline the total charge of the detected products and considering only events in which the charge of a heavy evaporation residue plus the sum of the charges of all detected light particles ($Z < 3$) accounted for almost the total charge of projectile plus target once corrected for the detector efficiency.

The second class of events, that is characterized by multiple-fragment emission, was selected by demanding more than two intermediate-mass fragments in the exit

channel at laboratory angles larger than 20° in coincidence with a heavy evaporation residue.

Identification of a clear evaporative component in the particle spectra at backward angles allowed, through a subtraction procedure, determination of the light charged-particle multiplicities for both the pre-equilibrium and the evaporative components of the spectra at all angles. This information was used to extract the excitation energy deposited into the compound nucleus. The selection of those events in which only light particles are produced allows the establishment of the excitation energy region in which the emission of heavier clusters sets in.

II. EXPERIMENTAL SETUP

The experiment was performed at the SARA coupled cyclotron facility in Grenoble, using a ^{32}S beam of 960 MeV, on an enriched (96%) ^{58}Ni target of $400 \mu\text{g}/\text{cm}^2$ thickness. Heavy fragments were detected in four large-area ($5 \times 5 \text{ cm}^2$) $300\text{-}\mu\text{m}$ -thick silicon detectors placed symmetrically on a cross around the beam axis with their centers at $\theta = 8^\circ$ at a distance of 140 cm from the target. The energy signal and the time of flight, measured with respect to the rf signal of the machine, allowed us to determine the masses of the products stopped in the silicon detectors. These trigger detectors were placed inside the 4π charged-particle detector system AMPHORA which, in the present configuration, consists of 140 CsI(Tl) crystals read out by photomultiplier tubes and located on 11 rings concentrically arranged at various distances from the target, covering all angles from 1.5° to 175° . For the elements of AMPHORA the pulse-shape discrimination method was used to identify charged particles with $Z = 1, 2$. Figure 1 shows an example of the identification pattern obtained with one of the modules, there is a rather good separation of H and He isotopes, and all fragments with $Z > 2$ are grouped in a region well separated from the alpha-particle line.

Information on the multiplicities of fragments with charge $Z > 2$ is possible with such a technique; however, the well-known Z dependence of the scintillation output of the CsI crystals changes the detection threshold for various fragments as a function of their charge. Moreover, the reaction kinematics plays an important role in our case since the motion of the center of mass (2.7 cm/ns) results in a rather large shift upward in the fragment energy spectrum at forward angles and in a very severe compression at backward angles so that a good fraction of the backward angle fragment yield might have energies that fall below the detection threshold. All these effects result in a charge- and angle-dependent efficiency for the detection of intermediate-mass fragments so that the condition imposed on their multiplicities (as described below) should be considered in fact as lower limits. Nevertheless, the device is still useful to reject peripheral collisions characterized by an energetic projectile-like fragment at forward angles whose energy is certainly above the detection thresholds.

No selection on the AMPHORA multiplicity signal was done at the acquisition level, the only requirement to

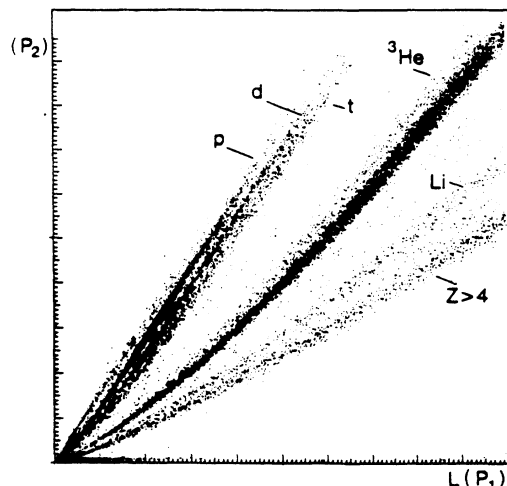


FIG. 1. Identification patterns obtained plotting the fast versus slow components of the CsI(Tl) light output.

record an event being the detection of a fragment with $Z > 2$ detected in one of the four trigger detectors.

The energy calibration of the silicon detectors was performed using α particles from radioactive sources (Am and Cm); the time of flight was calibrated using the ^{32}S elastic scattering peak clearly visible in the time spectrum. The CsI detectors were calibrated placing transmission surface barrier silicon detectors of various thicknesses ($20\text{--}1000 \mu\text{m}$) in front of one element of each ring of AMPHORA and recording singles events triggered by the firing of any one of the AMPHORA elements. Calibration of the selected CsI counters was deduced from the ΔE signals of protons and α particles traversing the transmission detectors using the energy-loss tables [13]. The cylindrical symmetry of the CsI detectors in each ring allowed derivation of the energy calibration for each element of the array.

III. RESULTS

A. Heavy fragments

According to the methods used in previous work [10] a selection based on the kinematical properties of the heavy fragments detected at forward angles was adopted to separate the evaporation residues from the rest of the reaction products. Figure 2 shows a mass versus velocity contour plot of such fragments detected on the four trigger counters centered at $\theta_{\text{lab}} = 8^\circ$. The peak visible at low masses around $V \sim 4 \text{ cm/ns}$ is actually an artifact due to the condition imposed on this spectrum that the fragment be stopped in the rather thin Si detectors, hence all the fragments with high velocity produced in very peripheral collisions are missing from Fig. 2. This condition does not affect the events enclosed in the triangle that have been initially associated with products originating from more central collisions.

The projections on the velocity and mass axes of such selected events are shown in Figs. 3 and 4, respectively.

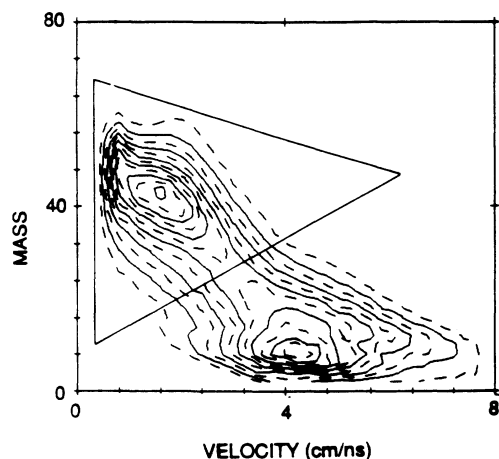


FIG. 2. Velocity versus mass contour plots of the fragments stopped in the trigger Si detectors at $\theta_{\text{lab}} = 8^\circ$.

The velocity distribution shows a rather broad bump which extends well beyond the center-of-mass velocity corresponding to full momentum transfer $V_{\text{FMT}} = 2.7$ cm/ns indicated by the arrow in the bottom of Fig. 3. The distribution of events exceeding V_{FMT} are compatible with the emission of large clusters from the composite system and are not reproducible with a calculation that includes only evaporation of light particles as it has been seen previously [11]. Moreover, Fig. 4 shows that the mass distribution of the considered fragments is centered around a value slightly lower than half the total mass of the system. Therefore the possibility that part of the measured fragment yield originates from binary fission events cannot be ruled out. In order to check this point we performed a kinematical calculation of the fission process based on a simple picture of linear momentum transfer (LMT) [14] and on systematics of total kinetic energy (TKE) [15].

The three arrows in the top part of Fig. 3 represent the first moments of the calculated velocity distribution of fission fragments detected at 8° assuming 50%, 70%, and

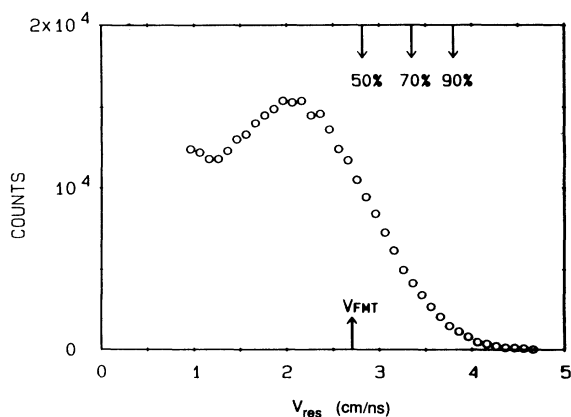


FIG. 3. Velocity distribution of the fragments detected at $\theta_{\text{lab}} = 8^\circ$ enclosed in the triangle shown in Fig. 2.

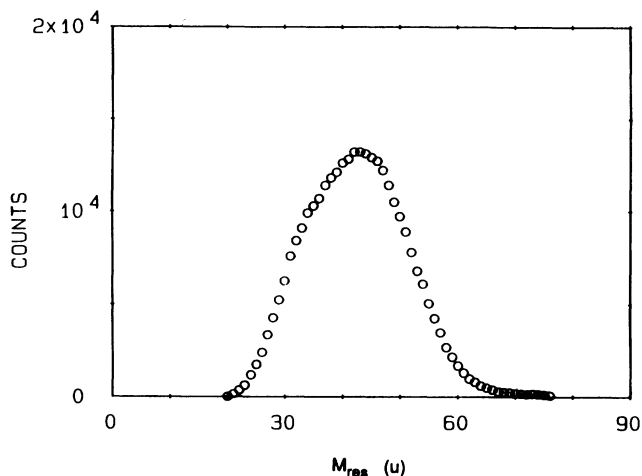


FIG. 4. Mass distribution of the fragments detected at $\theta_{\text{lab}} = 8^\circ$ enclosed in the triangle shown in Fig. 2.

90% LMT, respectively. One can see that the high-velocity side of the measured distribution is compatible with the kinematics expected for symmetric fission events following incomplete fusion.

These observations indicate that for the $^{32}\text{S} + ^{58}\text{Ni}$ system at $E_{\text{beam}} = 30$ MeV/nucleon a selection of evaporation residues based on the kinematics of the heavy fragments detected at forward angles is not unambiguous because of the similarities of their expected masses and velocities with those of asymmetric fission or deep-inelastic fragments. Therefore we made use of the 4π coverage of the AMPHORA detector to reconstruct on an event-by-event basis the total detected charge and thus to separate the different processes.

In Fig. 5 is shown the distribution of the total reconstructed charge of the products identified in our system defined as follows:

$$Z_{\text{tot}} = A_{\text{HI}}/2 + (2M_{\text{He}} + M_{\text{H}})\epsilon, \quad (1)$$

where A_{HI} is the mass of the heavy fragment detected at

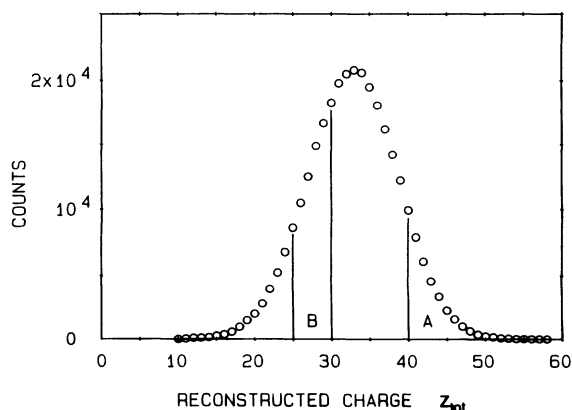


FIG. 5. Total reconstructed charge distribution using Eq. (1) (see text).

8° , M_{He} and M_{H} are the multiplicities of helium and hydrogen nuclei, respectively, detected in the AMPHORA system, and $\varepsilon=0.75$ is a factor that takes into account the geometric efficiency and the energy thresholds of the device for light particles. A Monte Carlo simulation containing the kinematics and the average multiplicities of the present experiment shows that multiple hits in a single element have a negligible effect on the response of the device. The quantity Z_{tot} represents therefore an estimate of the total charge carried by the heavy fragment plus all the light particles. It is accurate to about 4–5 units.

In Fig. 5 it can be seen that most of the events have a Z_{tot} smaller than the total charge of the system. The missing part corresponds to one or more undetected or unidentified fragments produced in the collision. The region labeled “B” in Fig. 5 has been selected as representative of events in which the average undetected charge amounts to about the Z_{HI} of the heavy fragment. For this class of events we proceeded to a further selection on the total multiplicity of light particles (M_{LP}) detected in AMPHORA. Demanding events in which $M_{\text{LP}} < 4$ one obtains the velocity spectrum shown in Fig. 6(b) (triangles) that clearly represents rather peripheral collisions in which little momentum is transferred and the undetected charge is probably bunched in a projectile-like fragment (PLF) traveling at very small angle. The squares in Fig. 6(b) represent the velocity spectrum of fragments in the class “B” events demanding $M_{\text{LP}} > 5$. These high-velocity–high-multiplicity events probably have their origin in more central collisions where a large amount of energy has been deposited in a system that deexcites by splitting into two or more fragments, one of which is detected by our trigger counters.

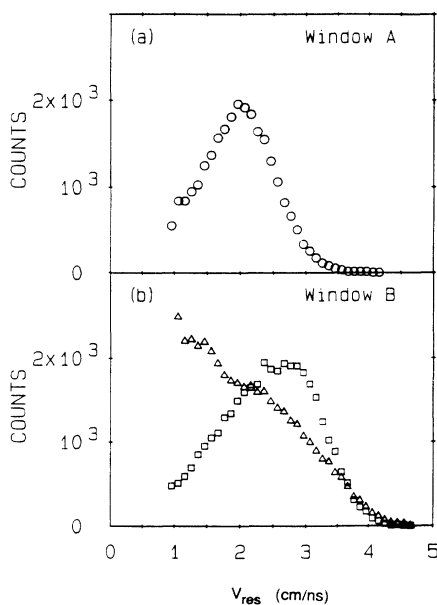


FIG. 6. Velocity distribution of fragments detected at $\theta_{\text{lab}} = 8^\circ$ for two selections of the parameter Z_{tot} (see text).

A second region labeled “A”, defined by $Z_{\text{tot}} > 40$, corresponds to events in which one heavy fragment has been detected in coincidence with light particles ($Z = 1, 2$) and essentially all the entrance channel charge has been reconstructed (more than 90%). In Fig. 6(a) is plotted the velocity distribution of heavy fragments for this class of events. Its Gaussian shape and the centroid at $V \sim 2$ cm/ns indicate that an incomplete fusion has taken place where, besides the evaporation residue, only light particles are produced both in the first stage of the reaction and in the subsequent decay. These events should correspond to rather central collisions in which the pre-equilibrium picture would describe the incomplete fusion process since events with production of projectile-like fragments are excluded. The compound nucleus thus formed deexcites by emission of light particles ($n, Z = 1, 2$).

B. Class “A” events: Fusion evaporation

This class of events has the nice feature of being produced in collisions where no clusters heavier than α particles are emitted, neither as PLF in the early stage of the reactions nor as statistically emitted fragments from the composite system, so one can make a rather accurate determination of the excitation energy deposited in the primary compound nucleus. In order to estimate the contribution to the total energy balance due to the pre-equilibrium particles, we subtracted from the total experimental spectra the “evaporative” component which was normalized at the most backward angles (where only such a component appears) and then projected to all other laboratory angles under the assumption of an isotropically emitting source with the compound nucleus velocity.

In Fig. 7 are presented energy spectra of H and He particles detected at all angles by the AMPHORA system in coincidence with evaporation residues. The solid lines represent the evaporative component described by a Maxwellian distribution in the center of mass of the emitter. The slope (representing the “average nuclear temperature” [16]) and the Coulomb barrier are free parameters fixed by the fit to the experimental spectra taken at $\theta_{\text{lab}} = 150^\circ, 117^\circ, \text{ and } 90^\circ$, whereas the velocity of the emitting source has been fixed equal to the measured evaporation residue (ER) velocity. One notices the well-known high-energy tail at the most forward angles that is not described by the single thermalized source which reproduces the backward H and He spectra.

We did not attempt to model this high-energy component of the spectra in terms of a second emitting source but assumed that they represent a pre-equilibrium particle emission removing momentum and excitation energy from the compound nucleus.

From energy conservation one can now determine the excitation energy deposited in the compound system as follows:

$$E_{\text{th}}^* = E_{\text{beam}} - \sum_{ij} \langle E_{ij} \rangle (dM_{ij}/d\Omega_j) \Delta\Omega_j - E_{\text{rot}} - E_{\text{kin}} + Q, \quad (2)$$

where E_{th}^* is the thermal excitation energy deposited into

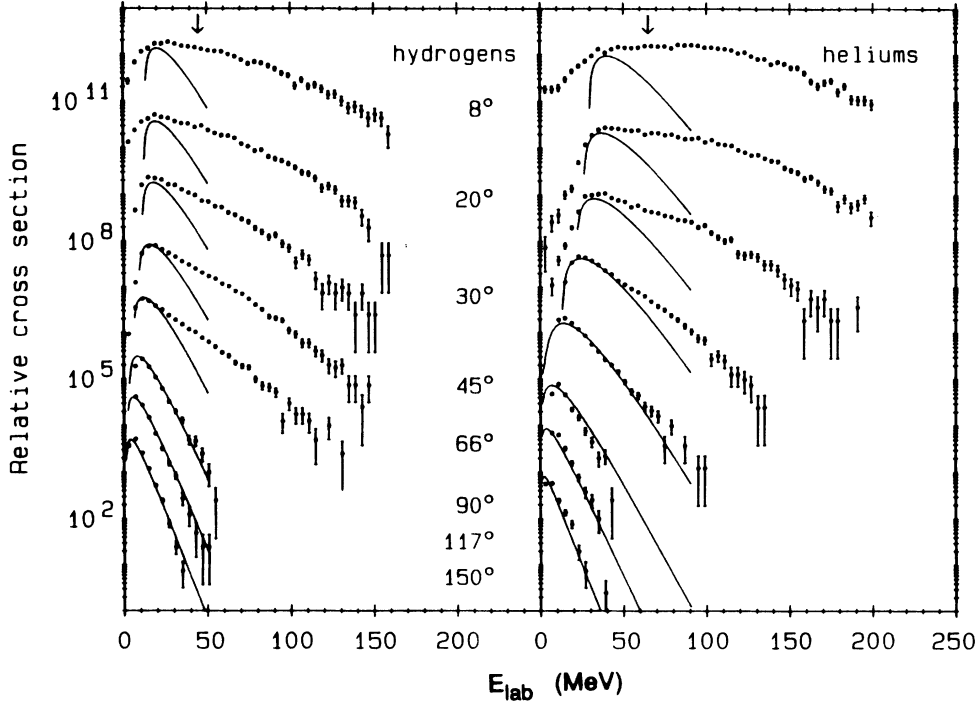


FIG. 7. Laboratory energy spectra of H and He particles at different angles.

the system, E_{beam} is the incident energy, the indices i and j indicate the particle kind and the angular position of the AMPHORA detectors, respectively, $\langle E_{ij} \rangle$ is the average energy of the pre-equilibrium component of the spectrum, $dM_{ij}/d\Omega_j$ is the differential multiplicity of the pre-equilibrium component, E_{rot} is the rotational energy of the compound system estimated from the average value of the spin distribution for fusion, E_{kin} is the kinetic energy of the recoiling compound system, and Q is the reaction Q value.

Since not all the detectors of AMPHORA have the same good isotopic separation for H and He, we have extracted the ^2H and ^3He contributions for both the evaporative and the fast components from a subset of good detectors. The contribution of ^3He on the He spectra is

negligible, while we had to take into account the ^2H contribution which represents about 30–40% of the pre-equilibrium H spectra and 15–20% of the evaporated H. The N/Z ratio of the system being very close to unity, it can be reasonably expected that the pre-equilibrium neutron emission has an energy spectrum, angular distribution, and multiplicity very similar to the proton case; consequently, one can take the neutron contribution equal to the proton one in the energy balance without introducing a large error. All the parameters used and extracted from this procedure are reported in Table I.

In order to cross check the global consistency of the method and the validity of our assumption on the neutron contribution we determined the velocity of the compound system after pre-equilibrium emission applying

TABLE I. Parameters extracted from the fitting procedure on the charged-particle spectra for the two considered classes of events. The errors on the quantities deduced from the fitting procedure correspond to a 100% variation in the χ^2 of the fit to the backward angles. The errors on the experimental masses represent the mass resolution of the Si detectors.

	Class "A" events	Multifragment	
M_{pe}^p	3.5 ± 0.5	2.6 ± 0.5	Pre-equilibrium H multiplicity
M_{pe}^α	2.7 ± 0.8	1.5 ± 0.7	Pre-equilibrium He multiplicity
V_{ER}	$2. \pm 0.09$	2.3 ± 0.09	Exp. residue velocity (cm/ns)
V_{CN}	1.98	2.31	Calc. CN velocity (cm/ns)
A_{ER}	49 ± 2.4	37 ± 2.4	Exp. ER mass (amu)
ϵ_{CN}^*	3.6 ± 0.2	5.3 ± 0.2	CN excit. energy (MeV/n)
M_{EV}^p	5.3 ± 0.7	3.7 ± 0.7	Evaporated proton multiplicity
M_{EV}^α	3.2 ± 1.3	2.3 ± 1.3	Evaporated α multiplicity
T_{EV}^p	$5. \pm 0.6$	$5. \pm 0.6$	Average proton temperature (MeV)
T_{EV}^α	6.1 ± 1.1	$6. \pm 1.4$	Average α temperature (MeV)

parallel momentum conservation and assuming equal contributions for protons and neutrons as follows:

$$M_p V_p = M_{CN} V_{CN} + \sum_{ij} M_i V_{ij} \cos\theta_j (dM_{ij}/d\Omega_j) \Delta\Omega_j, \quad (3)$$

where $M_p V_p$ is the projectile momentum, $M_{CN} = M_p + M_t - \sum_{ij} M_i (dM_i/d\Omega_j) \Delta\Omega_j$ is the compound system mass, $M_i V_{ij} \cos\theta_j$ are the pre-equilibrium particles' parallel momenta, and the indices i and j have the same meaning as in (2).

Since the sequential evaporation process is assumed to be isotropic in the center of mass of the emitting source [in our case the compound nucleus (CN)], from the central limit theorem of statistics one deduces that the ER's velocity distribution is a Gaussian centered around the value of the emitter's velocity [17]. The value of $V_{CN} = 1.98$ cm/ns obtained from (3) is then a good indication that our assumption on the pre-equilibrium neutron contribution is correct (see Table I).

In order to investigate the relationship between the ER velocity and the amount of linear momentum (excitation energy) transferred, the velocity distribution was cut into three slices. The fitting procedure to extract the evaporation and the pre-equilibrium components in the light-particle spectra was then repeated for the three velocity windows as in previous work [10]. It was found that such selection has an effect only on the kinematics of the evaporation process: In fact the high (low) velocity window is associated with an increased (decreased) yield of evaporated charged particles in the backward direction but the amount of pre-equilibrium particles is essentially unchanged. This indicates that the width of the ER velocity distribution for this rather light system is largely dominated by the kinematics of the evaporation process which greatly smears the relationship between the compound nucleus velocity and the ER velocity. With this in mind we proceeded to the comparison of these "average" events with the results of a statistical model calculation performed using the code CASCADE.

As input parameters for such a calculation we used the values of excitation energy, mass, and charge of the CN deduced experimentally after the pre-equilibrium stage of the reaction. Since all events that involve fission-like processes were experimentally rejected, the calculation was performed over an angular momentum range defined by a triangular distribution with $J_{\max} = J_{Bf=0}$, where $J_{Bf=0}$ represents the spin value at which the fission barrier vanishes for this nucleus.

It has been shown in recent work [10,11,16] that when the excitation energy of a medium mass nucleus exceeds about 1.5 MeV/nucleon the level density parameter "a" deduced from the simple Fermi gas formula $E^* = aT^2$ changes from the "low-temperature" value $a = A/8$ to about $a = A/13$. This has been explained for nuclei of mass $A = 208$ by the variation of the nucleon effective mass with temperature [18]. As a consequence, we have performed statistical model calculations using different values of the inverse level density parameter $K = A/a$ ranging from 8 to 14. The average values of temperatures and multiplicities for protons and α 's resulting from such calculations are listed in Table II.

A careful comparison of our results with the predictions of the statistical model goes beyond the aim of this work. However, it is interesting to notice that the agreement of the experimental temperatures and multiplicities with the calculated ones indicates that we have isolated a set of events in which a violent rather central collision takes place involving a substantial loss of nuclear matter and excitation energy due to pre-equilibrium emission and leading to the formation of a hot nucleus that reaches thermal equilibrium.

One also notices that the experimental average temperatures extracted from the α -particle spectra are higher than those deduced from the proton ones. These results confirm the trend already observed for the decay of $A = 160$ nuclei formed with large excitation energy [19] where it was shown that the "average temperature" extracted from the α spectra is closer to the "initial temperature" of the excited nucleus than the one extracted from the proton ones, thus suggesting that the two kinds of particles are emitted on the average at different steps of the decay chain.

C. Multiple fragment emission

The class of events described in the preceding section is compatible with a process of incomplete fusion involving rather central collisions (absence of projectile-like fragments) leading to the formation of a composite system with an average excitation energy of about 3.6 MeV/nucleon. Such a value is low compared to the total available center-of-mass energy of 6.9 MeV/nucleon for complete fusion.

If one retains the picture of a well-defined separation between the fast stage of the reaction and the deexcitation of a thermalized system, one can imagine that in the collisions a number of quasicompound nuclei are formed with a wide range of excitation energies due to fluctua-

TABLE II. Proton and α -particle temperatures and multiplicities predicted by the statistical model code CASCADE. The reported values are average over different calculations performed using an inverse level density parameter K ranging from 8 to 14. The errors indicate limits to the variation of the quantities in the range of K considered.

M_{EV}^p	4.8 ± 0.5	Average calculated proton multiplicity
M_{EV}^α	3.1 ± 0.5	Average calculated α multiplicity
T_{EV}^p	4.9 ± 0.2	Average calculated proton temperature
T_{EV}^α	5.9 ± 0.1	Average calculated α temperature

tions in the pre-equilibrium particle multiplicities and energies. According to the systematics of linear momentum transfer deduced from both ER velocity and fission fragment folding angle measurements [20] one would expect that at a bombarding energy of 30 MeV/nucleon the most probable value of LMT for central collisions lies between 70 and 80 % of the total and consequently in many cases the excitation energy deposited in the system should be higher than the value we find. With the rather severe selection performed in the preceding section a slice centered around 3.6 MeV/nucleon was cut in the excitation energy distribution, but at least two other decay channels could be envisaged besides the one analyzed: a fission (or deep-inelastic) channel and an evaporation involving clusters heavier than α particles in the cascade; one or both of these classes of events could originate from a different region of the excitation energy distribution.

As described earlier our experimental setup allows us to measure the mass and energy of one fragment and to detect the partner in a case of a fission event, but a precise angular distribution and energy measurement of the latter is not possible. Since this information is indispensable to identify the source of light-particle emission and deduce the excitation energy, we did not analyze this class of events.

We have, however, analyzed a second class of events in which a heavy fragment was detected in one of the trigger counters at $\theta_{\text{lab}}=8^\circ$ and two or more intermediate-mass fragments (IMF) with charge $Z_{\text{IMF}} > 2$ were detected in the AMPHORA array at angles larger than 30° . This choice of angular range has been suggested by the observation that while in the H spectra the pre-equilibrium component extends up to almost 90° , the fast source component of the He spectra is already very small at 45° and disappears at larger angles; consequently, one can reasonably assume that all heavier fragments detected beyond about 30° originate from a thermalized source.

As explained above we have no information on the exact charge and energy of the IMF's, the only information available being a lower limit of their multiplicity. Moreover, it was imposed that no fragment be detected at angles smaller than 30° (except the trigger one on the Si detectors); this filter assures that all peripheral collisions are rejected. For these events it was still possible to determine the excitation energy and momentum removal by pre-equilibrium particles with the same technique as for the previous class of events.

The parameters extracted from the subtraction procedure are shown in Table I; one notices that the pre-equilibrium multiplicity for both H and He particles is lower than before; as a consequence we find an excitation energy deposited into the system of 5.3 MeV/nucleon. The processes involving the emission of two or more IMF's are then associated with a different region of the excitation energy distribution in agreement with the results obtained in multiple-fragment coincidence measurements of Ref. [22]. From Table I one can see that for this class of events the average temperature of evaporated protons and α 's remain essentially unchanged (within error bars) compared to the previous case, suggesting that

the clusters are emitted on the average early in the deexcitation chain; a similar effect has been found in the $^{32}\text{S} + ^{\text{nat}}\text{Ag}$ reaction at 30 MeV/nucleon described in Ref. [11].

IV. DISCUSSION

With the use of the 4π detector AMPHORA we were able to measure the excitation energy of a composite system formed in incomplete fusion processes in central collisions of $^{32}\text{S} + ^{58}\text{Ni}$ at 30 MeV/nucleon. For such a light system the kinematical effects due to the large amount of emitted particles are rather severe; one can notice from Fig. 8 that the angular distributions of pre-equilibrium particles are rather wide implying a large amount of perpendicular momentum removed by these particles. As a consequence, a simple picture of participant-spectator model assuming beam velocity and beam direction for the pre-equilibrium particles leads to an overestimate of the excitation energy deposited into the incomplete fusion nucleus. Moreover, as discussed above, the relationship between the compound nucleus and the ER's velocity is almost washed out by the subsequent evaporation process (this effect being more severe the lighter the evaporation source). In our case the excitation energy of the incomplete fusion nucleus was determined by subtracting the energy of the pre-equilibrium particles measured at all angles and yields a value substantially smaller than that reported for the same system in Ref. [23] where the same quantity was deduced from a participant-spectator model through the measure of the ER's velocity.

From the analysis of the two classes of events so far discussed we have extracted only average values of the

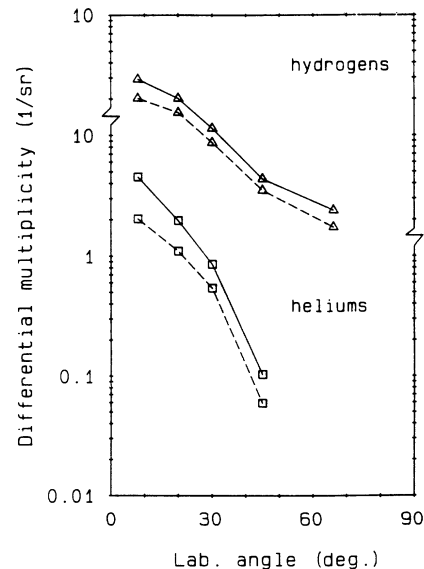


FIG. 8. Angular distribution of the pre-equilibrium component of H and He particle spectra; the solid and dashed lines (to guide the eye) correspond to the class "A" and the multifragment class of events, respectively.

excitation energy deposit since both the fast and the “thermal” components of the light-particle spectra have a continuous distribution overlapping to a large extent; consequently, the subtraction of the pre-equilibrium contribution cannot be done on an event-by-event basis. Nevertheless one notices that the “thermal” component of the spectra at forward angles shows a rather steep fall and consequently all the light particles whose energies fall above the arrows indicated in Fig. 7 can be reasonably attributed to the fast stage of the reactions.

With this assumption one can select events with different amounts of pre-equilibrium emission using the multiplicities of light particles with energy larger than the indicated arrows. Such a selection was done on the α particles which are responsible for a large part of the excitation energy removed from the composite system.

We then counted the number of events associated with n He particles in the high-energy side of the spectra with $n=0,1,2,\dots$; the subtraction procedure described above was then applied to these events allowing us to determine the corresponding excitation energy of the compound nucleus. Increasing the factor n by one unit corresponds to augmenting the pre-equilibrium particle multiplicities and consequently the excitation energy deposit decreases accordingly; in order to obtain statistically significant spectra for the fitting procedure the value of n was never larger than 3. Therefore, with a few points it was possible to extract the trends of the excitation energy distributions associated with our two deexcitation modes plotting the number of events of each class for different values of n .

In order to make a quantitative comparison of our data with model predictions one should have a measurement of the absolute cross sections for both kinds of events considered. In our case the fragment trigger counters were positioned only at one angle ($\theta=8^\circ$); consequently, lacking an angular distribution we could not obtain the integral cross sections. Moreover, in the analysis of our second event types we rejected all events in which a projectile-like fragment was detected at forward angles regardless of its energy; in this way all the events involving statistical emission of IMF's in the forward direction were also rejected. As a consequence, both a relative normalization between the two kinds of processes analyzed and an absolute cross section estimate cannot be drawn from our data. It is nevertheless interesting to compare the trends of the excitation energy distributions associated with the two kinds of deexcitations with the predictions of the statistical multifragmentation model of Ref. [21].

In Fig. 9(a) the prediction of such a model is plotted for a nucleus of mass $A=74$ populated at various excitation energies with the same probability. The dashed line represents the relative yield of decays involving the emission of one large cluster and a number of fragments with mass $M < 5$ (essentially nucleons and α particles). These events (called by the authors “pseudoevaporation residues”) are well suited to compare to our class “A.” The solid line represents the yield of events involving at least three fragments of mass $A_f > 5$ and a number of light particles ($M < 5$) in the exit channel and can be compared

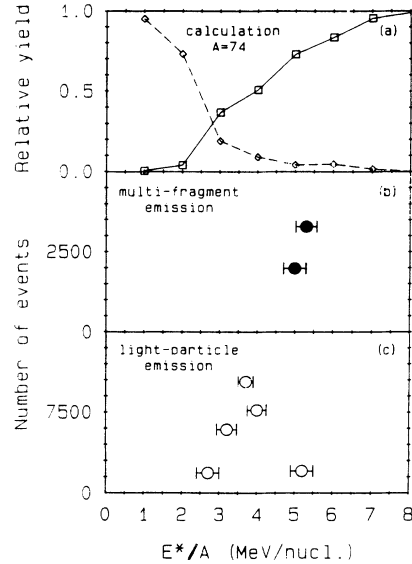


FIG. 9. (a) Calculated relative yield of two decay modes for an $A=74$ nucleus as a function of excitation energy per nucleon (Ref. [21]). (b) Relative cross sections for multiple-fragment emission events as a function of excitation energy. (c) Same as above for class “A” events. See text for details.

with our second class of events. The experimental points plotted in Figs. 9(b) and 9(c) represent the excitation energy distributions relative to our two event types.

One notices that the evaporation events involving only light-particles emission (open symbols) have a decreasing probability as one increases the excitation energy in agreement with the predictions (the rightmost experimental point was extracted imposing $n=0$ with the additional condition that there are no high-energy H); events involving multiple-fragment emission (solid symbols) take over above a certain excitation energy and show an increasing probability in good agreement with the model.

On the low-energy side of Fig. 9(c) one can notice that the experimental distribution decreases while the calculated one increases; this apparent disagreement is due to the fact that our analysis is confined to rather central collisions since we have rejected all events in which a projectile-like fragment is produced; such events are expected to be associated with the lowest excitation energy deposit.

V. CONCLUSIONS

We have measured mass and velocity distributions of heavy fragments detected in coincidence with light charged particles produced in central collisions in the reaction of $^{32}\text{S}+^{58}\text{Ni}$ at 30 MeV/nucleon. As a result of the use of the 4π charged-particle detector AMPHORA we were able to select events in which only light particles are emitted in the first stage of the reaction; consequently, after subtraction from the spectra of the “thermal” component it was possible to measure the average energy carried by such fast emitted particles and thus to evaluate the excitation energy associated with two distinct classes

of events. Exploiting the large fluctuations both in energy and in multiplicity of the pre-equilibrium process we could determine the trend of the excitation energy distributions associated with (a) events in which a “conventional” evaporation takes place after incomplete fusion and (b) three or more intermediate-mass fragments are found in the exit channel. Although we cannot determine the absolute yields of the two processes, one can nevertheless observe from the excitation energy dependence of the relative cross sections that for this system above an excitation energy of about 4 MeV/nucleon the emission of several fragments becomes the dominant decay mode.

A qualitative agreement with a statistical multifrag-

mentation model and the almost constant value of the temperatures deduced from the light-particle spectra suggest that the fragments are emitted early in the deexcitation cascade; nevertheless, from our data we cannot establish a precise time scale for such processes.

ACKNOWLEDGMENTS

We thank the SARA staff for providing good quality beams and for their excellent support during the run. This work was supported by the INFN, the U.S. Department of Energy under Grant DE-FG05-86ER40256, the Robert A. Welch Foundation, and the CNRS-IN2P3.

-
- [1] P. J. Siemens, *Nature* **305**, 410 (1983).
 - [2] G. Bertsch and P. J. Siemens, *Phys. Lett.* **126B**, 9 (1983).
 - [3] L. P. Csernai and J. I. Kapusta, *Phys. Rep.* **131**, 223 (1986).
 - [4] J. P. Bondorf, R. Donangelo, I. N. Mishustin, C. Pethick, and K. Sneppen, *Phys. Lett.* **150B**, 57 (1985).
 - [5] D. H. E. Gross and X. Z. Zhang, *Phys. Lett.* **161B**, 47 (1985).
 - [6] C. Barbagallo, J. Richert, and P. Wagner, *Z. Phys. A* **324**, 97 (1986).
 - [7] S. Levit and P. Bonche, *Nucl. Phys.* **A437**, 426 (1985).
 - [8] J. P. Bondorf, in *Proceedings of the Workshop on High Resolution Heavy Ion Physics at 20–100 MeV/u*, edited by M. Martinot (DPh N/MF, Saclay, 1978), p. 37.
 - [9] M. Blann and B. Remington, in *Proceedings of the Texas A&M Symposium on Hot Nuclei*, edited by S. Shlomo, R. P. Schmitt, and J. B. Notowitz (World Scientific, Singapore, 1988), p. 145, and references therein.
 - [10] K. Hagel *et al.*, *Nucl. Phys.* **A486**, 429 (1988).
 - [11] R. Wada *et al.*, *Phys. Rev. C* **39**, 497 (1989).
 - [12] D. Drain *et al.*, *Nucl. Instrum. Methods* **A281**, 528 (1989).
 - [13] L. C. Northcliff and R. F. Schilling, *Nucl. Data Tables* **A7**, 233 (1970).
 - [14] V. E. Viola, B. B. Back, K. L. Wolf, T. C. Awes, C. K. Gelbke, and H. Breuer, *Phys. Rev. C* **26**, 178 (1982).
 - [15] V. E. Viola, *Nucl. Data* **A1**, 391 (1966).
 - [16] G. Nebbia *et al.*, *Phys. Lett. B* **176**, 20 (1986).
 - [17] J. Gomez del Campo, R. G. Stokstad, J. A. Biggerstaff, R. A. Dayras, A. H. Snell, and P. H. Stelson, *Phys. Rev. C* **19**, 2170 (1979).
 - [18] P. F. Bortignon and C. H. Dasso, *Phys. Lett. B* **189**, 381 (1987).
 - [19] M. Gonin *et al.*, *Phys. Lett. B* **217**, 406 (1989).
 - [20] V. E. Viola, *Nucl. Phys.* **A502**, 531c (1989), and references therein.
 - [21] Sa Ben-Hao, B. H. Sa, Y. M. Zheng, and X. Z. Zhang, *Nucl. Phys.* **A509**, 499 (1990).
 - [22] See, e.g., L. G. Moretto *et al.*, in *Proceedings of the XXIX International Winter Meeting on Nuclear Physics*, edited by I. Iori (Bormio, Italy, 1991), p. 204.
 - [23] W. Bohne, H. Morgenstern, K. Grabisch, T. Nakagawa, and S. Proschitzki, *Phys. Rev. C* **41**, R5 (1990).